ORIGINAL ARTICLE

Contribution of water geochemistry and isotopes (δ^{18}O, δ^{2}H, ^{3}H, ^{87}Sr/^{86}Sr and δ^{11}B) to the study of groundwater flow properties and underlying bedrock structures of a deep landslide

M. Deiana[1] · M. Mussi[2] · M. Pennisi[2] · M. Boccolari[1] · A. Corsini[1] · F. Ronchetti[1]

Abstract

A comprehensive understanding of bedrock lithology and groundwater circulation is necessary to identify areas prone to landslide initiation and reactivation. This necessity is particularly required in the case of outcroppings of weak rocks such as gypsum that, due to their high solubility and low mechanical strength, can promote slope deformation with the development of caves and collapses. In the Upper Secchia River Valley, where gypsum outcrops extensively and is covered by landslide deposits, an accurate identification of the gypsum outcrops and their distribution is needed to reduce the damage to urbanized slopes. In this paper, a hydrologic and geochemical approach is used in the Montecagno landslide to identify the origin, flow paths and transit time of groundwater circulating inside the landslide body and to identify gypsum deposits and their distribution in the bedrock. The results of groundwater-level monitoring, δ^{18}O-δ^{2}H and ^{3}H isotope analyses and FLOWPC modelling suggest a local and recent origin of the groundwater hosted in shallow flow paths inside the landslide. Chemical and isotope (^{87}Sr/^{86}Sr, δ^{11}B) analyses offer evidence of the presence inside the landslide of small blocks of gypsum that, due to their dimensions, probably have a minor influence on landslide stability. This research demonstrates that the methodology used can provide satisfactory information about bedrock structures and their hydrological aspects.

Keywords Landslide · Isotopes · Groundwater · Triassic evaporite · Bedrock structure

Introduction

Landslides are a common hazardous phenomenon occurring in mountain chains. Bedrock lithology, together with rainfall infiltration and groundwater paths, is considered a main parameter in landslide initiation and kinematics; different lithotypes exhibit different geotechnical properties. Weak rocks can promote the development of failures, collapses and landslides. Accordingly, comprehensive knowledge of the aerial and underground distributions of weak rocks (evaporites, marls, and clays) is required to identify the main areas subjected to deformation.

Evaporite formations are typically considered weak rocks (Yılmaz 2001). Gypsum is characterized by high solubility and low mechanical strength and is commonly associated with other soluble minerals, such as anhydrite, calcite, and dolomite. These characteristics, together with a high degree of tectonization, can lead to collapse and the development of large depressions, fissures or caves (Chiesi and Forti 2009; Gutiérrez 2010; Gutiérrez and Cooper 2013) that can play a double role in the stability of rocks. On the one hand, they drain the groundwater hosted in a slope and produce an increasing slope stability factor; on the other hand, they lead to the development of collapses that can provoke slope deformation or produce damage to the infrastructure in the affected area.

Evaporite units underlie approximately 25% of the continental rocks of the earth (Klimchouk et al. 1996; Gutiérrez et al. 2013) and are often the bedrock of overlying formations (Denchik et al. 2019). Several evaporite outcrops are

✉ M. Deiana
manuela.deiana@unimore.it

1 Department of Chemical and Geological Sciences, University of Modena and Reggio E., Via Campi, 103, 41125 Modena, Italy

2 Institute of Geosciences and Earth Resources, CNR, Via G. Moruzzi, 1, 56124 Pisa, Italy

scattered across Italy from the Alps to Sicily with gypsum units cropping out from or lying beneath unconsolidated cover (Forti and Sauro 1996; Klimchouk et al. 1996; Chiesi et al. 2010; Calligaris et al. 2017).

In the northern Apennines, outcrops of Triassic evaporites are very common and in particular are widely distributed in the USRV (Fig. 1). Triassic evaporites outcropping locally in the USRV consist mainly of metre- to decametre-scale gypsum, anhydrite, black dolomite and minor halite (Lugli 2001). Layers of dolomitic clasts within a carbonatic matrix are locally detected. In northern Italy, many cases of deformation promoted by evaporite collapses that involve anthropic housing and infrastructure have been reported (Buchignani et al. 2008; Intrieri et al. 2015; La Rosa et al. 2018). For this reason, the underground distribution of gypsum units and evaporites in general is important since the presence of fissures or caves in the bedrock can influence the stability of the overlapping formations with the development or reactivation of landslides (Gutiérrez and Cooper 2013). Gypsum units outcropping along the USRV are commonly covered by slope debris or landslide deposits. An accurate identification of gypsum outcrops and their extents is needed to understand the destabilizing role that gypsum may play in slope debris or landslides and to identify areas that are prone to collapse.

In addition, to get a better understanding of the stability/instability conditions of slope debris/landslides, a clear identification of the recharge area, the groundwater origin and the residence time is required. In recent decades, new and indirect methods (based on water chemistry and isotopes) have been used to better understand groundwater processes in unstable slopes (de Montety et al. 2007; Cervi et al. 2012; Vallet et al. 2015; Marc et al. 2017; Deiana et al. 2018) and to demonstrate the existence of lithologies and structures that are not visible with surface-based geological investigations (Bogaard et al. 2007).

This paper focuses on the landslide affecting the urbanized Montecagno slope (northern Apennines of Italy). The landslide at the sliding surface depth exhibits a cyclic and seasonal deformation pattern that is correlated with seasonal groundwater variations inside the landslide body (Deiana et al. 2017). Moreover gypsum formations outcrop along the Montecagno slope, but their exact distribution is not well known. Stratigraphic information obtained during borehole drilling is available only for some points (P1–P12) (Fig. 1).

To fill in the lack of information on the bedrock lithology in the other portions of the landslide, and clarify relations between groundwater circulation and bedrock lithology in the Montecagno landslide new investigations based on a coupled hydrologic and geochemical approach were performed.

Specifically, the study aims to clarify performing the following aspects:

- define the origin, flow paths and transit time of groundwater circulating inside the landslide body using groundwater level monitoring, $\delta^{18}O$-δ^2H and ^3H isotope analyses and FLOWPC modelling (Malozweski and Zuber 2002);
- investigate evidence of gypsum deposits inside the landslide body using water chemistry (main ions) and isotopes ($^{87}Sr/^{86}Sr$, $\delta^{11}B$) and highlight the main reactivating factor acting on montecagno landslide mechanism.

Study area

Hydrogeological and hydrochemical setting

The study site is located in the USRV in the northern Apennines of Italy.

The northern Apennines are a fold and thrust mountain belt made up by sedimentary rocks, many of which are turbidite sequences (flysch rock masses) and clayey chaotic deposits (clayshales, marls) (Fig. 1b). The complex structural features of outcropping formations, the high degree of tectonization and the wide presence of faults prevent the development of a regional deep flow path developed in this portion of the mountain chain. Only in some limited portion in the east part of the Apennines chain, where thick permeable rock masses with lateral continuity outcrops, a deep regional flow is discovered (Gargini et al. 2008; Cervi et al. 2014). In the research area, groundwater flow is limited at the slope scale, where permeable rock masses or slope deposits outcrops and shallow unconfined aquifers develop (Segadelli et al. 2017; Deiana et al. 2017; Tazioli et al. 2019). Only at the bottom of the Secchia Valley where Evaporite Triassic rocks outcrops with a certain lateral continuity a deep flow path is developed (Colombetti and Fazzini 1987; Chiesi et al. 2010) (Fig. 1b).

Hydrochemical features of groundwater hosted in this portion of the Apennines mainly depend by water–rock interaction with outcropping formations (Cervi et al. 2012). Specifically groundwater discharging by evaporitic formations are characterized by Ca-SO$_4$ hydrofacies with Sr and B contents lower than 15 mg L^{-1} and 2 mg L^{-1}, respectively (Toscani et al. 2001; Duchi et al. 2005). Groundwater interacted with flysch formations or clay-rich formation mainly belong to Ca-HCO$_3$ hydrofacies with a low ion contents and Sr and B values normally lower than 1 mg L^{-1} and 0.05 mg L^{-1} (Cervi et al. 2012).

Study site

The studied landslide is located at elevations ranging between 1050 and 800 m a.s.l. (Fig. 1). It consists of an earth/debris slide (Cruden and Varnes 1996) and covers an
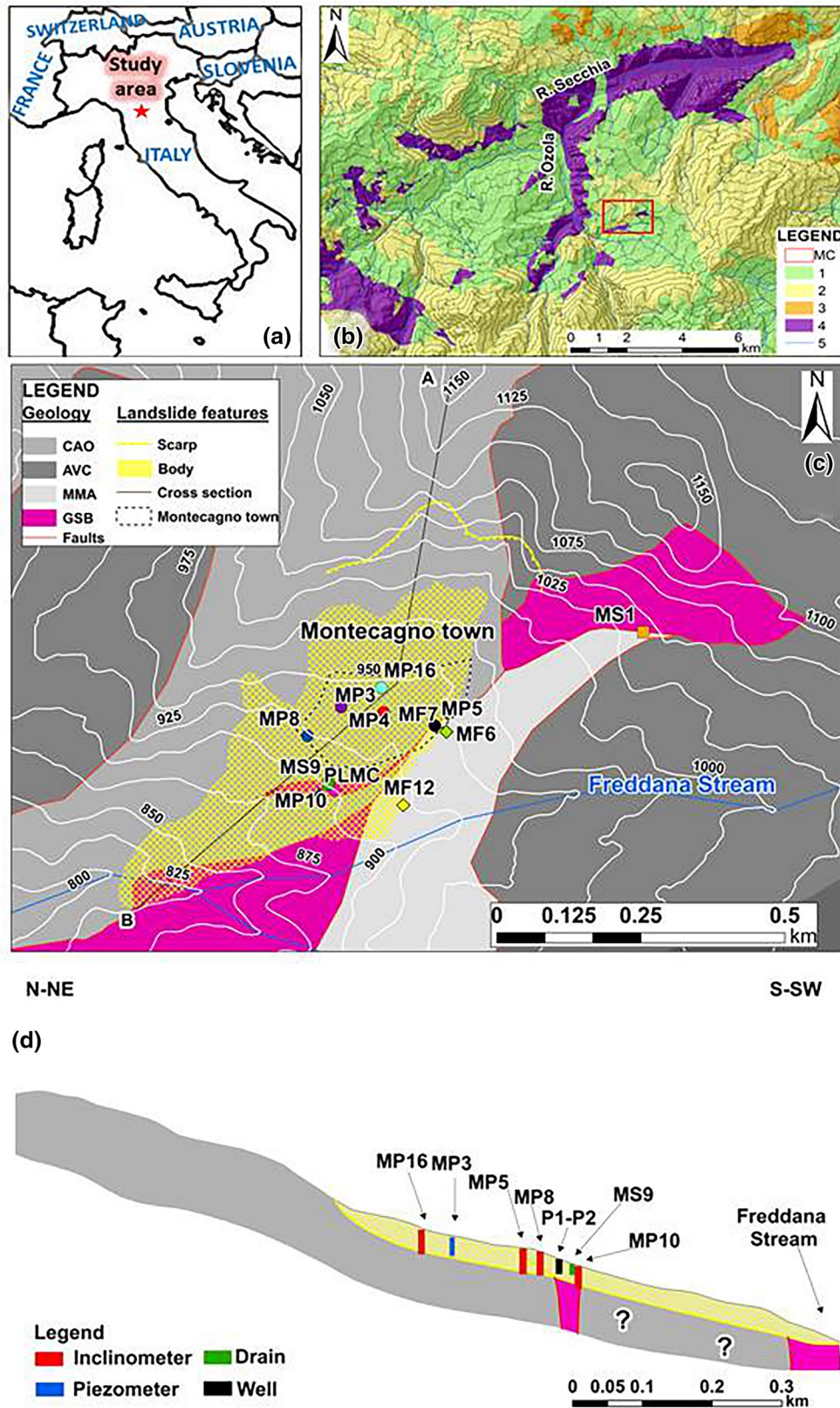
Fig. 1 **a** Geographic location of the study site; **b** distribution of gypsum in the USRV and location of study site. MC, Montecagno Landslide, 1 impermeable rock masses, clayey, marls etc.; 2 medium-low permability rock masses, flysch; 3 medium-high permeability rock masses, sandstones, limestone; 4 high-permeability karstified rock masses; 5 river/torrent; **c** geological sketch map of the Montecagno study site; **d** cross-section of the Montecagno slope

area of 0.2 km^2, while the mean thickness of the sliding mass is 28 m. The total estimated volume of the landslide is 3.6 Mm^3, and the mean deformation velocity is 2.4 mm month^{-1}.

The activity of the landslide is related with the seasonality of the groundwater level variation which is strictly related with the rainfall pattern of the area. During the summer and dry periods when the groundwater depth in the piezometer is normally higher than 5.2 m below the ground surface (b.g.s.) the landslide velocity is near to zero. In the humid seasons, when in the same piezometer the groundwater depth is around or lower than 4 m b.g.s., the landslide starts to accelerate and the velocity reacts or exceeds 3 mm month^{-1} (Corsini et al. 2013; Deiana 2017). Along the slope, four sedimentary geological formations outcrop (Fig. 1). The geological formations consist of evaporitic and clay-rich rock masses that exhibit a marked structural complexity and a large lithological heterogeneity. Along the slope, the following geological formations outcrop (from the bottom to the top): (1) a gypsum formation (GSB-Upper Triassic); (2) a shale with limestone formation (AVC-Lower Cretaceous); (3) a flysch formation (CAO-Upper Cretaceous); and (4) a marls formation (MMA-Oligocene).

The GSB formation is composed mainly of gypsum alternating with layers of anhydrite and highly fractured black dolomite. Locally, layers of dolomitic clasts within a carbonate matrix with an Oligocene–Miocene tectonic origin are present. The AVC formation consists of clayey shale alternating with carbonatic, pelitic and marly layers. Locally, layers of calcareous clasts are encompassed within a clayey matrix outcrop. The MMA formation is composed mainly of marls and pelitic marls with local layers of sandstone and clayey shale, especially at the bottom of the formation. The CAO flysch formation is composed mainly of a calcareous-marly component, but locally, arenaceous-pelitic layers can alternate with layers made by centimetric clasts in a clay matrix.

All the geological formations are characterized by a high degree of tectonization with several faults.

The slope is bordered downward by a water body, the Freddana stream that is oriented in a NE–SW direction in the study area. The discharge pattern of the Freddana depends mainly on the distribution of precipitation throughout the year.

Clay-rich formations and deposits, namely, the AVC and MMA formations, are considered aquicludes. Flysch and evaporite formations, namely, the CAO and GSB formations, are considered to be aquifers or aquitards due to their medium–low permeability (Gargini et al. 2008), which is the result of a medium–high degree of fracturing.

Along the Montecagno slope, a contact spring (Fetter 1980), namely, MS1, is detected at the bottom of the GSB slab that outcrops in the northeast portion of the study area. This spring, which drains a catchment area composed of the GSB slab tectonically overlapping the AVC formation, shows low discharge values depending on the distribution of precipitation throughout the year.

Boreholes drilled into the landslide area have been equipped with one standpipe piezometer (MP3) and five inclinometers (MP4, MP5, MP8, MP10, and MP16) (Table 1; Fig. 1).

Two well screens were performed along the slope and transverse to the landslide to reduce the groundwater level

Table 1 List of the selected surface and groundwater monitoring points

Type	Name	Geological formation involved[a]	Elevation m a.s.l.	Maximum watershed elevation (m a.s.l.)	Piezometer/inclinometer depth (m from ground surface)	Piezometer slotting depth (m from ground surface)
Spring	MS1	GSB	1050	1150		
Ditch	MF2	CAO	985	1170		
Piezometer	MP3	CAO	960	1170	30	From 2 to 28
Inclinometer	MP4	CAO	959	1170	29	
Inclinometer	MP5	CAO	948	1170	35	
Ditch	MF6	CAO-MMA	950	1170		
Ditch	MF7	CAO-MMA	949	1170		
Inclinometer	MP8	CAO	939	1170	29	
Drain system	MS9	CAO-GSB (probably)	920	1170		
Inclinometer	MP10	CAO-GSB (probably)	920	1170	30	
Ditch	MF12	CAO-MMA	925	1170		
Inclinometer	MP16	CAO	966	1170	34	
Rainfall collector	PLMC		920	1170		

For each points the geological bedrock and ground elevation is reported. The total length of inclinometer and piezometer is reported as well as the depth of the slotted part of the piezometer. The maximum ground elevation of the watershed is reported for each points

[a]Geological formations: GSB gypsum formation, CAO flysch formation, MMA marly formation

inside the slope deposits. The wells are linked underground, and the endpoint of the drain system is represented by MS9, which collects groundwater coming from the entire landslide body (Fig. 1).

Close to MS9 at the same elevation, a rainfall collector PLMC was installed to collect rainfall (Fig. 1).

The mean annual rainfall during the monitoring period (2013–2016) was 1730 mm (ARPAE-RER). The observed rainfall distribution is reported in Fig. 2. Frequent snow events occurred from November to March, and each single event accumulated up to 100 cm of snow on the ground surface. The mean annual air temperature during the monitoring period was 10.5 °C; the coldest month was February, and the warmest month was July (Fig. 2).

According to Thornthwaite and Mather (1957), the average annual effective rainfall is 1240 mm.

Methods

To identify the geology of the bedrock and the hydrogeological features of the landslide, a multidisciplinary study was performed on the Montecagno landslide and the surrounding area.

To consider the groundwater variation inside the landslide, the groundwater level and discharge were monitored using a piezometer, a broken inclinometer and a drainage system between 2014 and 2016.

The $\delta^{18}O$–δ^2H signatures were characterized every 4 months between 2014 and 2018 and coupled with the ^3H content and FLOWPC modelling to assess the groundwater origin and flow paths to obtain a semi-quantitative evaluation of the groundwater transit time inside the landslide. The chemistry, $^{87}Sr/^{86}Sr$ ratios and $\delta^{11}B$ values were determined

to investigate the water–rock interaction processes of the groundwater along the flow paths.

## In situ activities

Groundwater level monitoring

One borehole in the landslide was equipped with a standpipe piezometer (Table 1); this piezometer, MP3, is located in the central part of the landslide at an elevation of 960 m a.s.l. and is slotted from 2 to 28 m below the ground surface (Fig. 1). In MP3, a CTD-Diver (Eijkelkamp) was used to continuously acquire groundwater level data with a frequency of 1 h from January 2015 to April 2016; non-continuous groundwater level monitoring was performed monthly (every 3–4 months) from January 2014 to April 2016.

The other five boreholes were equipped with inclinometers, but in a few cases, the inclinometers were destroyed by landslide deformation. After a preliminary investigation, the inclinometers were cut and highly deformed, and they worked almost similarly to piezometers. For this reason, at these points (MP4, MP5, MP8, MP10, and MP16), non-continuous groundwater level monitoring was performed monthly (every 6 months) from January 2014 to June 2015 (Fig. 1).

During October 2011 and July 2015, two well screens were created along the landslide at elevations of 932 and 928 m a.s.l. to reduce the groundwater level along the slope.

The wells (diameter: 1 m, depth: 15 m) were linked underground and collected groundwater from the entire landslide. The endpoint of this drain system is represented by MS9, located at 920 m a.s.l. (Fig. 1, Table 1). In MS9, discharge was monitored continuously from January 2015 to May 2016 using an OTR water level probe installed in 2015;

Fig. 2 Monthly pattern for total rainfall, effective rainfall and temperature in the period September 2013-November 2016 recorded in the Ligonchio weather station
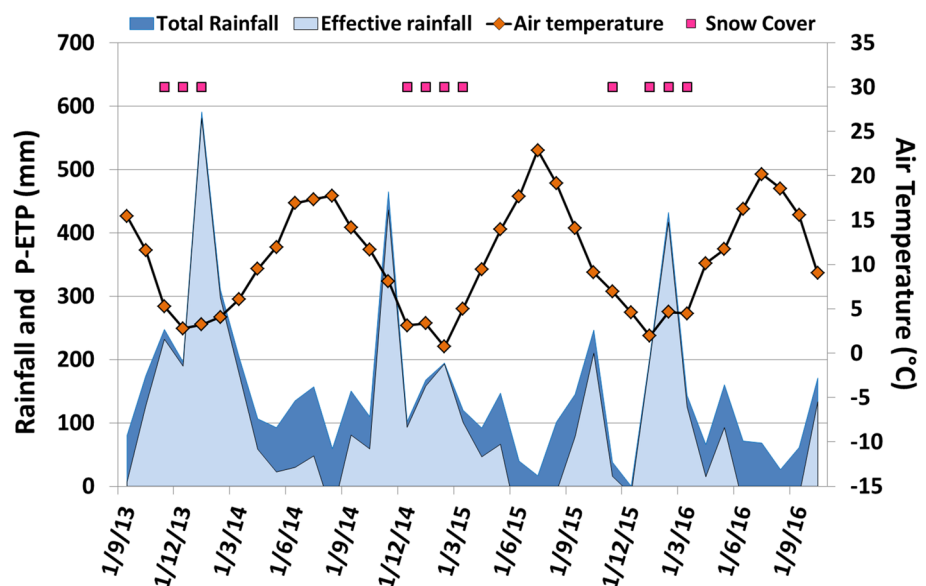
the frequency of the readings was every 1 h. Moreover, non-continuous measurements of discharge using a graduated container were performed monthly (every 4 months) from January 2014 to January 2015 and daily (every 20 days) from February 2015 to June 2016.

Surface and groundwater sampling

To collect groundwater and surface water samples for chemical and isotopic analyses, 2–30 sampling campaigns were performed between January 2014 and March 2018 at the Montecagno study site. The sampling locations are presented in Fig. 1. Sampling locations were selected to obtain representative samples of surface water and groundwater both inside (MP3, MP4, MP5, MP8, MS9, MP10, and MP16) and outside (MS1, MF2, MF6, MF7, and MF12) the landslide; the sampling sites were associated with different geological formations outcropping in the study area (Table 1). For comparison, sampling sites located outside the landslide were also included in this study. The rainfall collector, which was located at 920 m a.s.l. (PLMC; Fig. 1), collected water for chemical and isotopic analyses from January 2016 to January 2018.

Moreover, during the monitoring period, four springs (S1, S2, S3 and S4) located approximately 0–20 km away from the study area were selected to monitor the stable isotopic composition of the water (δ^{18}O-δ^2H). These springs were selected because the features of their hydrogeological catchments were consistent with the isotopic characteristics determined by Vespasiano et al. (2015). Specifically, they have small and well-defined recharge areas as well as small differences between the infiltration/recharge elevations and the spring elevations. For this reason, these selected springs contributed to obtaining a valid ^{18}O-elevation relationship and more representative background isotopic values in subsurface and surface water in the area, consistent with recent studies (Lauber and Goldscheider 2014; Vallet et al. 2015; Marc et al. 2017; Deiana et al. 2018).

Samples from springs, ditches and drain systems were collected directly from discharge points, whereas groundwater was collected from piezometers and broken inclinometers using a bailer or a low-flow pump (0.1 L s^{-1}), which occurred after removing three aliquots from the water volume contained in the piezometer.

Water samples were collected at a mean frequency of 4–6 months using 500 mL polyethylene (PE) bottles with double caps. The samples were filtered through a 0.45-μm cellulose membrane filter, and the aliquots used for cation analysis were acidified with Suprapur Merck 65% HNO$_3$. For all water samples, temperature (T), electrical conductivity (EC) and pH were measured in the field using a Crison MM40$^+$ multimeter equipped with a Ross glass electrode to measure pH. In addition, at two points (MP3 and MS9),

continuous EC and water T monitoring were performed from February 2015 to November 2016 using a CTD-Diver datalogger. The CTD-Diver allowed the measurement of the water temperature with a range of -20 to 80 °C, an accuracy of ± 0.1 °C, and a resolution of 0.01 °C. The EC was measured with a range of 0–120 mS/cm, an accuracy of $\pm 1\%$ and a resolution of $\pm 0.1\%$.

Water samples for stable isotope analysis (δ^{18}O, δ^2H) were collected at a mean frequency of 3 months using 50 mL PE bottles with double caps. Water samples for ^{3}H analysis (collected in 2 L PE bottles with double caps) were collected during four sampling campaigns in January, March, May and November 2015. Water samples for ^{87}Sr/^{86}Sr and δ^{11}B analyses were collected during a single campaign in November 2015 using 500 mL PE bottles with double caps. Samples collected for isotopic analysis were stored at 4 °C to avoid evaporation after collection.

Analytical methods

Chemical analyses on the water samples collected at the selected monitoring points in the Montecagno study site are reported in the Supplementary material (Table SM1).

Chemical analyses

Chemical analyses were performed at the Department of Chemical and Geological Sciences at the University of Modena and Reggio Emilia and the Chrono-Environment Laboratory at the University of Franche-Comté.

An inductively coupled plasma spectrometer (ICP-AES Perkin Elmer Optima 4200) was used for the analysis of Ca, Mg, Na, K, Sr, and B$_{tot}$. Anion (SO$_4$, Cl, NO$_3$) concentrations were assessed using high-pressure ion chromatography (Dionex DX 100). Total alkalinity (expressed in HCO$_3$) was assessed using the Gran titration method (Gran 1952). The total relative uncertainty was less than 5%. Silica was analysed with a Spectroquant spectrophotometer (Pharo 300, Merck) using a silica test kit (Merck). A total of 29 chemical analyses were completed during this study.

Isotopic analyses

The results of the isotopic investigations conducted from 2014 to 2018 are shown in Table S1 (Supplementary material).

The isotopic compositions of the water molecules were measured in water collected from all sampling locations at a mean frequency of 3 months; notably, the ^{18}O/^{16}O ratio was determined in 106 samples using an IRMS spectrometer, and the ^{2}H/^{1}H ratio was determined in 88 samples using a Los Gatos Research liquid water isotope analyser LGR-LWIA-24d. Isotopic analyses were performed at the IGG-CNR,

Pisa. The results are reported as δ-‰, which reflects deviations from the standard isotopic value (V-SMOW). The analytical precision is ± 0.10‰ and ± 1.0‰ for $\delta^{18}O$ and δ^2H, respectively.

The ^3H content was measured using a PerkinElmer Quantulus liquid scintillation counter based on the electrolytic enrichment method. The results are reported as tritium units (T.U.). The analytical precision is better than 0.8 T.U.

The $^{87}Sr/^{86}Sr$ ratio was measured in 5 samples in November 2015 using a Finnigan MAT 262 multi-collector mass spectrometer, which occurred after performing the ion-exchange separation of Sr from the matrix. The measured $^{87}Sr/^{86}Sr$ ratios were normalized to $^{86}Sr/^{88}Sr = 0.1194$. The reproducibility of the measured $^{87}Sr/^{86}Sr$ ratios was tested using replicate analyses of the NIST SRM 987 ($SrCO_3$) standard; during the analytical period, this standard yielded an average value of 0.710237 ± 0.000020 (2SD, $n = 6$).

The $\delta^{11}B$ value was determined using an MC-ICP-MS Neptune Plus with a combination of internal standardization and bracketing standards for instrumental mass bias correction; this instrument can achieve precision for isotope ratio measurements in the range of 0.001–0.002%.

Data integration and analysis

Lumped parameters modelling (FLOWPC)

FLOWPC is a software program based on lumped parameter models applicable to the interpretation of environmental tracers in groundwater systems (Maloszewski and Zuber 2002; Viville et al. 2006; Sànchez-Murillo et al. 2015). In this study, the $\delta^{18}O$ isotopes of rainwater and groundwater collected from the landslide are processed to obtain information about the turnover time (Maloszewski and Zuber 2002), and the groundwater flow inside the landslide is evaluated using a combined method made by a piston flow model (PFM) and an exponential model (EM). In the PFM, the flow lines are assumed to have the same transit time, and hydrodynamic dispersion and diffusion are negligible (Maloszewski and Zuber 2002). In the EM, the flow lines are assumed to have an exponential distribution of transit times, and no exchange of tracers between the flow lines happens (Maloszewski and Zuber 2002). This method allows us to obtain a semi-quantitative evaluation of the groundwater transit time inside the landslide.

Results

Groundwater level, EC and T

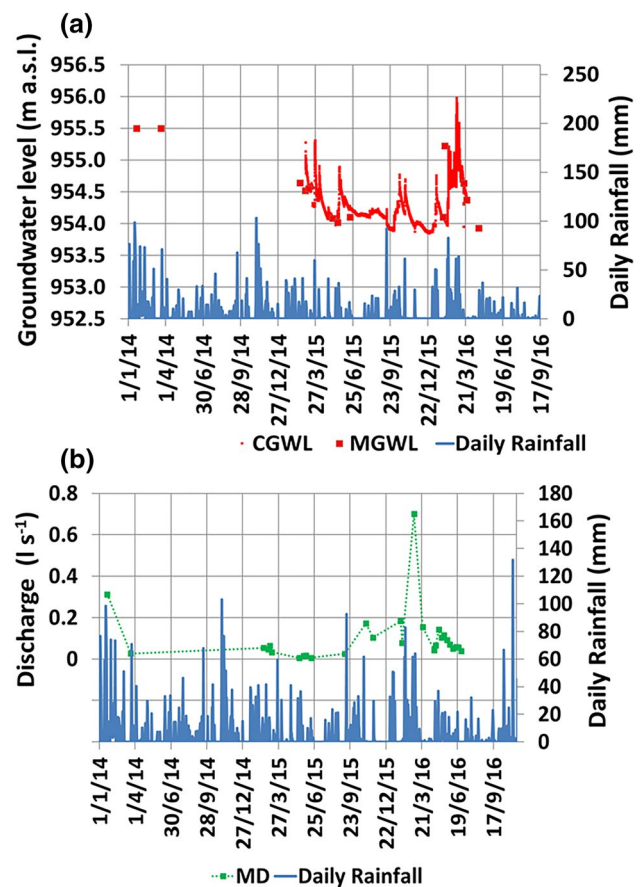The results of the groundwater level monitoring in MP3 are reported in Fig. 3 and Table 2.

Fig. 3 **a** Groundwater level compared with daily rainfall in MP3; **b** discharge compared with daily rainfall in MS9

Table 2 List of manual groundwater level monitoring (expressed in m a.s.l.) performed using piezometer and broken inclinometers

Point	21/1/14	21/3/14	11/3/15	18/6/15
MP3	955.5	955.5	954.6	954.1
MP4		936.4	937	931.6
MP5	943.3		946.5	946.5
MP8				917.8
MP10				911
MP16		961.7	957.9	958.9

During the monitoring period, the groundwater level in MP3 ranged between a minimum value of 953.9 m a.s.l. recorded at the end of the summer period (September 2015) and a maximum value of 955.9 m a.s.l. recorded during winter (February 2016). The temperature ranged between 10.2 °C and 11.6 °C; the EC varied between 600 μS cm^{-1} and 1400 μS cm^{-1}.

In MS9, the discharge ranged between 0.7 L s^{-1} recorded during winter (March 2016) and 6.0E−4 l s^{-1} recorded during summer (June 2015). T ranged between

10.5 and 11.5 °C; the EC varied between 700 and 1400 $\mu S\ cm^{-1}$.

The groundwater level measured in the broken inclinometers (Table 2) ranged between a minimum value of 934.7 m a.s.l. (MP4) and a maximum value of 961.8 m a.s.l. (MP16).

Water chemistry

The results of the water chemistry analyses are reported in Fig. 4 (see also Supplementary material).

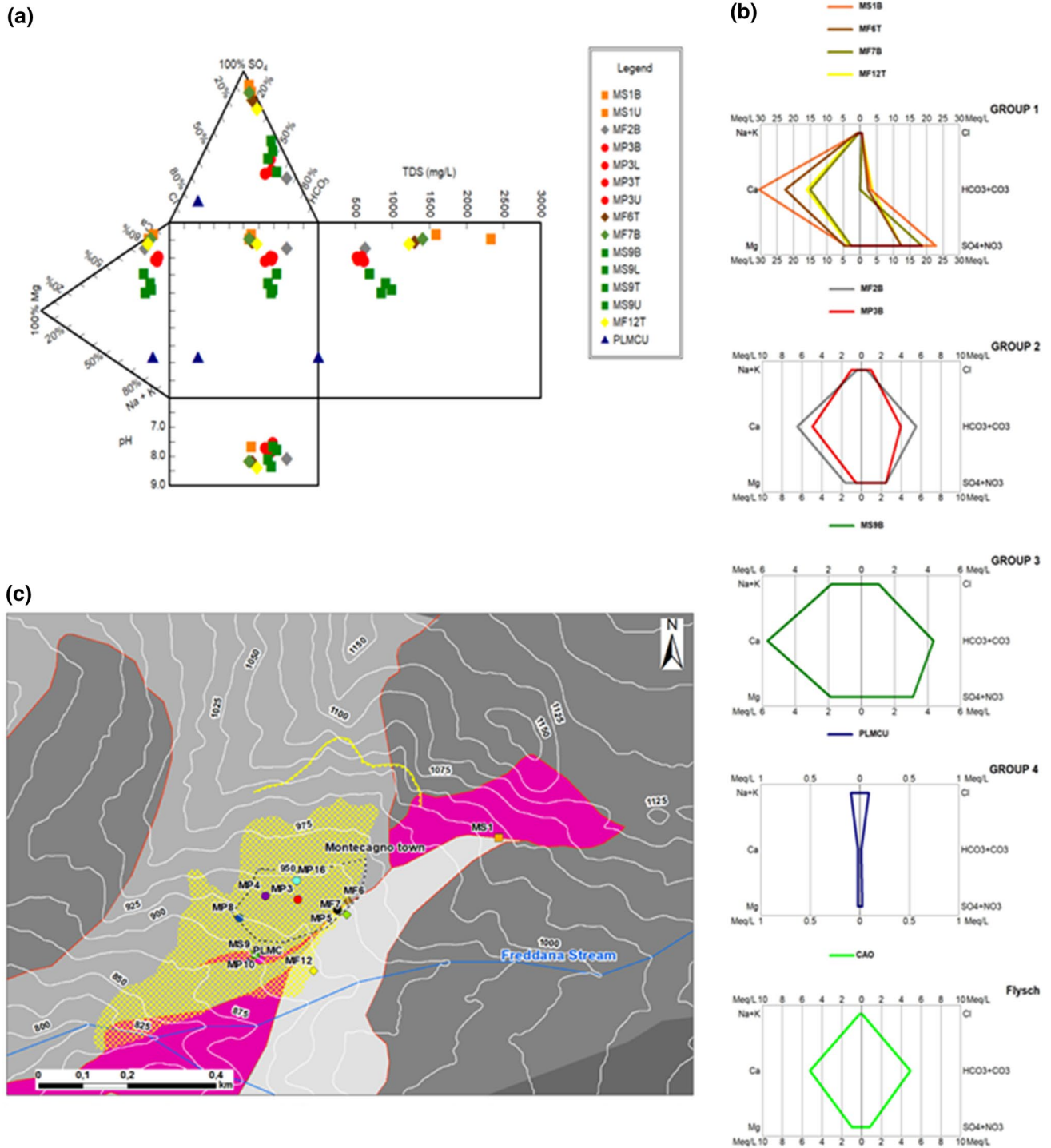In the landslide and surrounding areas, four different groundwater hydrotypes are identified.

Fig. 4 **a** Durov diagram of hydrochemical analyses; **b** stiff diagrams of representative samples; **c** spatial representation of sampled points

Group 1 corresponds to Ca-SO$_4$-rich water and includes MS1, MF6, MF7 and MF12. Samples belonging to this group show high contents of Ca (up to 610.4 mg L^{-1}) and SO$_4$ (up to 1493 mg L^{-1}). Low contents are detected for Na (mean value 13.2 mg L^{-1}), K (mean value 6.8 mg L^{-1}) and Cl (mean value 14.5 mg L^{-1}). Variable contents are detected for HCO$_3$ (ranging from 132 to 320 mg L^{-1}) and Mg (ranging from 2.3 to 66.0 mg L^{-1}). The EC varies between 996 and 2570 μS cm^{-1}. The mean pH value is 8.0, and the mean T value is 10 °C.

Group 2 corresponds to Ca-HCO$_3$-rich water and includes MF2, MP3, MP4, and MP10. Samples belonging to this group predominantly comprise Ca (up to 235.6 mg L^{-1}) and HCO$_3$ (up to 336 mg L^{-1}). Cations Mg, Na, and K show mean values of 12.0, 16.5, and 8.2 mg L^{-1}, respectively, and non-negligible amounts of SO$_4$ and Cl are detected in MP3 (up to 200 and 35.9 mg L^{-1}, respectively). The EC varies between 536 and 985 μS cm^{-1}. The mean pH value is 7.6, and the mean T value is 12.7 °C.

Group 3 corresponds to Ca-HCO$_3$-SO$_4$-rich water and includes MS9. More specifically, water belonging to this group exhibits high concentrations of both HCO$_3$ (mean value of 323 mg L^{-1}) and SO$_4$ (mean value of 228 mg L^{-1}). Ca and Na are the most abundant cations (mean values of 129.4 and 55.1 mg L^{-1}, respectively). Subordinate concentrations are detected for Mg and Cl (mean values of 22.6 and 29.0 mg L^{-1}, respectively). Variable concentrations are detected for K (ranging from 7.9 to 40.1 mg L^{-1}). The EC varies between 1034 and 1255 μS cm^{-1}. The mean pH value is 7, and the mean T value is 12.4 °C.

Group 4 is represented by rainfall with main components of Na (1.7 mg L^{-1}), K (0.7 mg L^{-1}) and Cl (3.3 mg L^{-1}) corresponding to Na–K–Cl-rich water.

The sample CAO reported in Fig. 4 is an external spring collected in a carbonate flysch (Deiana et al. 2018) and is assumed to be an end-member of the water–rock interaction with the carbonate flysch.

Water isotopes (δ^{18}O-δ^{2}H, ^{3}H, ^{87}Sr/^{86}Sr, δ^{11}B)

The results of the isotopic analyses are reported in Table SM1 (Supplementary material) and Fig. 5.

The isotopic values of water from the Montecagno sampling points are reported in the δ^{18}O-δ^{2}H plot. In general, samples fall between the northern Italy meteoric water line (NILM) and the global meteoric water line (GMWL) and identify a best-fit line with the equation δ^{2}H = 7.96* δ^{18}O + 9.45 (r^2: 0.98).

The δ^{18}O and δ^{2}H isotopic compositions of the spring and surficial water range from − 10.25‰ (MS1) to − 8.85‰ (MF7) and from − 70.1‰ (MS1) to − 60.6‰ (MF7), respectively. The standard deviations of the isotopic values are higher than 0.29‰ (δ^{18}O) and 2.30‰

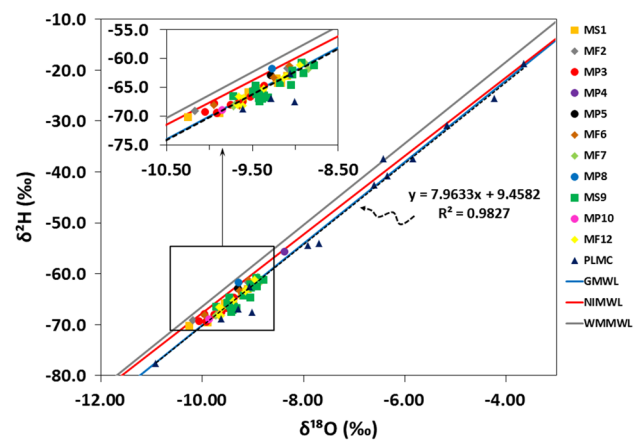**Fig. 5** δ^{18}O-δ^{2}H diagram. All water samples and rain samples are reported as well meteoric line valid for Western Mediterranean area (WMWL; Celle-Jeanton et al. 2000), North Italy (NIMWL; Longinelli et al. 2003) and Global line (GMWL; Craig 1961). Dashed black line corresponds to the calculated Local Line

(δ^{2}H); the coefficient of variation (CV, Koch and Link 1971) is 4.1% (δ^{18}O) and 5.2% (δ^{2}H).

During the monitored period, springs S1, S2, S3, and S4 showed δ^{18}O values ranging from − 10.25 to − 8.47‰ and δ^{2}H values ranging from − 69.1 to − 54.5‰. At each site, the standard deviation of isotopic values measured on differing dates ranges from 0.06 to 0.3‰ (δ^{18}O) and from 0.6 to 2.3‰ (δ^{2}H). The CV is 1.9% (δ^{18}O) and 2.3% (δ^{2}H). The mean values of the isotopic content and the standard deviations of S1, S2, S3, and S4 are reported in the Supplementary material in Table SM2. In groundwater collected from piezometers, drains and broken inclinometers, the δ^{18}O values range from − 10.05‰ (MP3) to − 8.13‰ (MP4), while δ^{2}H values range from − 69.4‰ (MP3) to − 55.6‰ (MP4). In groundwater, the standard deviations of the δ^{18}O and δ^{2}H values are lower than 0.27‰ (δ^{18}O) and 2.03‰ (δ^{2}H) and the CV is 0.9% (δ^{18}O) and 2.2% (δ^{2}H).

Rainfall collected by PLMC shows δ^{18}O values ranging from − 10.91 to -3.63‰ and δ^{2}H values ranging from − 77.6 to − 18.7‰. The standard deviation is 2.2 (δ^{18}O) and 18.2 (δ^{2}H); the CV is 29.8% (δ^{18}O) and 37.1% (δ^{2}H).

To identify the altitude of infiltration of precipitation in the study area, a δ^{18}O-elevation relationship was determined using springs MS1, S1, S2, S3, and S4 and following the approach proposed by Mussi et al. (1998) and Vespasiano et al. 2015. These selected springs, located 0–20 km around the study site, are used as natural pluviometer (Doveri and Mussi 2014; Cervi et al. 2016; Vespasiano et al. 2015; Deiana et al. 2018; Tazioli et al. 2019) as they are characterized by small, geologically defined catchment areas, and small differences between the elevations of maximum recharge and discharge points.

The relationship obtained for the Montecagno area is characterized by an isotopic gradient of $-0.44‰/100$ m (r^2: 0.98; not shown), which allows an estimation of the infiltration altitude of the groundwater inside the landslide. Infiltration altitudes consistent with the main elevation of the area were obtained for MP3 (1174 m a.s.l.), MS9 (1084 m a.s.l.), MP5 (1084 m a.s.l.) and MP8 (1086 m a.sl.). Inconsistent values were estimated for MP4 (852 m a.s.l.) and MP10 (1215 m a.s.l.). However, these points are associated with broken inclinometers in which groundwater circulation does not occur easily, such as in a piezometer. The broken inclinometers could have affected the isotopic compositions. Accordingly, these samples will not be considered in further discussions.

The isotopic gradient of $-0.44‰/100$ m is higher than the regional gradient of $-0.22‰/100$ m obtained for northern Italy (Longinelli and Selmo 2003) and is probably due to local effects at the slope scale, as recently described in other case studies in the northern Apennines (Deiana et al. 2017, 2018).

The results obtained using FLOWPC modelling and the combined PFM-EM method on $δ^{18}O$ values were selected using the sigma criterion-based approach (Malozweski and Zuber 2002). In this approach, the goodness of fit of a model is defined by a variable, namely, sigma, and the goodness of fit increases with a decrease in the sigma value. For the modelling performed in the Montecagno study site, the lowest sigma value obtained was 0.52, which is consistent with a turnover time (Tt) of 90–100 days.

The ^3H content was assessed in surficial water and groundwater by four sampling campaigns during 2015. During the first campaign, which was performed in January, a ^3H content of $3.9 ± 0.6$ TU was measured in MS1. In March, values of $4.3 ± 1.0$ TU and $4.3 ± 0.6$ TU were measured in MP3 and MS9, respectively. In May, the following ^3H contents were measured: $4.1 ± 0.7$ TU (MS1) and $3.7 ± 0.7$ TU (MP3). In November, the following ^3H values were measured: $5.1 ± 0.7$ TU (MP3), $4.0 ± 0.6$ TU (MS9), $3.2 ± 0.6$ TU (MF6) and $4.2 ± 0.7$ TU (MF12).

The $^{87}Sr/^{86}Sr$ ratio was assessed in November 2015. The $^{87}Sr/^{86}Sr$ value of spring MS1 was 0.70797. In ditches MF6 and MF12, $^{87}Sr/^{86}Sr$ values of 0.708083 and 0.708024, respectively, were measured. Groundwater collected inside the slope debris showed $^{87}Sr/^{86}Sr$ values of 0.708151 (MP3) and 0.708400 (MS9).

The $δ^{11}B$ contents, which were assessed in November 2015, are as follows: $16.84 ± 0.1$ (MS1), $7.24 ± 0.5$ (MP3) and $21.75 ± 0.4$ (MS9).

Discussion

Groundwater origin, flow paths and transit time

Changes in the groundwater level and pore pressure are crucial for the stability of a landslide. Groundwater hosted inside a landslide usually has a meteoric origin and responds to rainfall patterns. In the northern Apennines, however, recent studies have highlighted the presence inside the landslide of groundwater characterized by a deep origin (Cervi et al. 2012), by a long transit time and by deep flow paths in which the pressure transfer prevails over the mass transfer (Deiana et al. 2018).

In the Montecagno study site, the results show that a relevant portion of the landslide is saturated. The groundwater level inside the landslide deepens westward. In general, variations in the groundwater level over time suggest that rainfall patterns influence the groundwater level. However, in the left portion of the landslide, groundwater seems to be more static (0.20 m of variation in the groundwater level) than in the central and right portions, in which variations up to 3.8 m are measured.

The $δ^{18}O$-$δ^2H$ results support a meteoric origin of the groundwater in all the sampled sites. Seasonal variations are evident in almost all samples with the more depleted values measured at the beginning of spring (March 2014) and the heaviest values measured in autumn (November 2015). In the northern Apennines, autumn 2015 was particularly dry (300 mm of cumulative rain), and the main precipitation events happened after the end of summer. This could explain the heaviest isotopic values measured in this period.

The more depleted values in the area are measured in the upper portion of the slope and in the head zone of the landslide, specifically in MS1 ($-10.25‰$) and MF2 ($-10.17‰$) while the heavier values are measured in MP4 ($-8.13‰$ and $-8.37‰$) in a lateral portion of the landslide. The high variability of the isotopic composition measured in general the head zone of the landslide (MF2, $δ^{18}O$ CV: 5.6%) is probably correlated with the presence of shallow circuits directly recharged by precipitation (PLMC, $δ^{18}O$ CV: 29.8%). The presence of scarps and fracture promotes infiltration in this portion of the landslide. Lower variability is measured in the central and lower portions of the landslide (MP3, MS9). In this portions the stability of isotopic values ($δ^{18}O$ CV of 0.9%) highlights that groundwater is hosted in deeper and longer circuits in which the integration of the precipitation isotopic signal by the aquifer is promoted.

As supported by $δ^{18}O$-elevation relationship, groundwater shows a local origin. The infiltration altitudes obtained using the $δ^{18}O$ signatures for MS9, MP5 and

MP8 are consistent with the elevation of the area and of the main scarp and, for the lower portion of the landslide, exclude water sources other than local meteoric recharge. In particular, in MP3, the infiltration altitude (1174 m a.s.l.) almost coincides with the highest peak of the area, confirming a local recharge that involves the entire upper portion of the slope (Fig. 10).

Moreover groundwater hosted inside the landslide has a recent origin. The ^3H content measured in groundwater from both shallow and deeper hydrological circuits (3.8 TU and 4.3 TU, respectively) is close to the ^3H content recorded in springs from the northern Apennines (4.2 TU) sampled in the same period (Deiana et al. 2016, 2017). The groundwater turnover time, estimated by the PFM-EM model, is 177 days; this suggests that in the Montecagno landslide meteoric water takes approximately 6 months to infiltrate and circulate after being finally discharged from the landslide body.

Distribution of the evaporite bedrock under the landslide and mixing processes

Along the Montecagno slope, gypsum, flysch and clay formations outcrop. Specifically, flysch and clay formations outcrop continuously along the slope; gypsum formations outcrop in two different and separated parts: the first one in the upper portion of the slope and the second one in the lower portion of the slope. During the borehole execution, gypsum blocks were found below the lower portion of the landslide (corresponding to MS9 and MP10). However, the landslide affects the slope from 1050 m a.s.l. to the stream at 800 m a.s.l. Because of the landslide deposits, the nature of the bedrock and the lateral continuity of the gypsum blocks below the lower portion of the Montecagno landslide remains unclear. The presence of gypsum below and inside the landslide can influence the stability of the landslide body (Elorza and Santolalla 1998; Gutierrez 2010; Gutierrez et al. 2013); indeed, by means of fissures and fractures, gypsum can promote the drainage of groundwater hosted inside the landslide body and increase the stability of the slope. Moreover, the ongoing dissolution affecting gypsum can promote the enlargement of fractures and caves and increase the possibility of collapses. Additionally, the stability of the slope is influenced by the dimensions of the gypsum blocks; decametric blocks can have a greater influence and can affect a larger portion of the slope than blocks with other dimensions.

The aspects of the subsurface bedrock structure and the extent of the geological formation composing the bedrock of the Montecagno landslide were investigated and clarified using chemical analyses (Bogaard et al. 2007) and $^{87}Sr/^{86}Sr$–$\delta^{11}B$ analyses. The chemical analyses seem to suggest the presence inside the landslide of water–rock
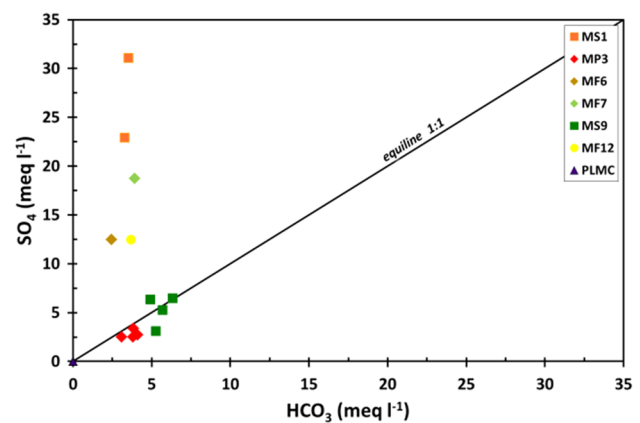
Fig. 6 Plot of HCO_3 vs SO_4 content in sampled groundwater
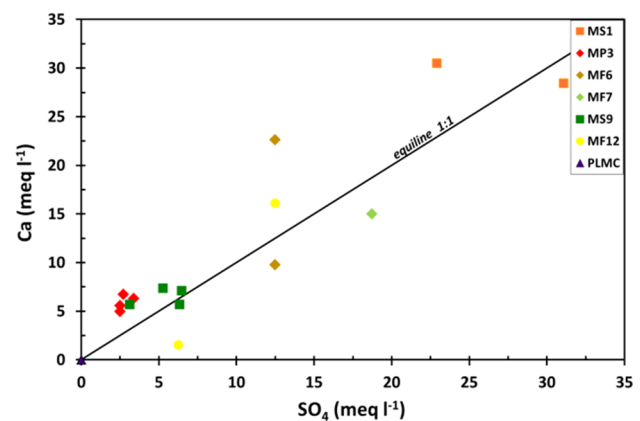
Fig. 7 Plot of Ca vs SO_4 content in sampled groundwater. The equiline indicates the gypsum equilibrium line

interaction processes involving gypsum formation. The predominant role of gypsum dissolution process is highlighted especially in the lateral portion of the landslide (MF6, MF7 and MF12 are positioned under the equiline, Fig. 6). In the central and lower portions of the landslide (represented by MP3 and MS9, respectively), the position of these points in Fig. 6 (very near to the equiline) suggests that groundwater could interact with both carbonate and gypsum materials. Specifically in the central portion of the landslide (MP3, above the gypsum equilibrium line) water–rock interaction with carbonate material seems to be the main process affecting groundwater. The occurrence of water–rock interaction with gypsum is likely the main processes affecting groundwater in the lower portion of the landslide (Fig. 7). Moreover in this part, chemical features of groundwater are probably affected secondly by mixing processes between a Ca-SO_4 end-member (MS1), a Ca-HCO_3 end-member (MF2-MP3) and a Na–K–Cl end-member (PLM). The Ca-HCO_3 groundwater that characterizes the upper portion of the landslide (MP3), moving into hydrological circuits toward the lower
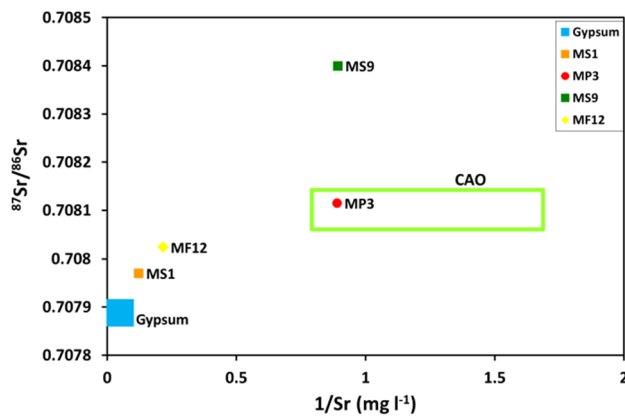
Fig. 8 1/Sr vs ^{87}Sr/^{86}Sr plot; gypsum field is by Dinelli et al. (1999). Note: CAO data are by Deiana et al. (2018)

Fig. 9 ^{87}Sr/^{86}Sr vs ^{11}B/^{10}B plot. Evaporites field is by Négrel et al. (2009), Elderfield (1986); carbonate field is by Négrel et al. (2009), Millot et al. (2011); rainwater by Négrel et al. (2007), (Xiao et al. 2013). Seawater is by Millot et al. (2011)

portion becomes enriched in SO_4 content. The increase in SO4 content is promoted by ditches that laterally bordered the landslide.

A further contribution is related with the preferential infiltration of rainfall, that is promoted by an upper secondary landslide scarp and contribute to the increasing of Na and K (Fig. 4a, b) in the lower portion of the landslide.

Data provided by ^{87}Sr/^{86}Sr seem to support the presence of water–rock interactions with gypsum in the lower portion of the slope (Fig. 8). In Fig. 8, end-members for the Triassic gypsum (Dinelli et al. 1999) and flysch (i.e., CAO) formations (Deiana et al. 2018) are reported. Groundwater from MS1 has ^{87}Sr/^{86}Sr ratios that match those of its evaporitic host rocks; the ^{87}Sr/^{86}Sr signature for MS1 is very similar to that reported for Triassic gypsum both in northern Apennines (Dinelli et al. 1999) and in Alps (Spötl and Pak 1996). The ^{87}Sr/^{86}Sr value measured in the lateral portion of the landslide (MF12), slightly higher than that of MS1, indicates a dominant interaction with gypsum and a subordinate influence of flysch formation (CAO). In the central portion of the landslide (MP3) the ^{87}Sr/^{86}Sr signature matches the CAO ^{87}Sr/^{86}Sr value (Fig. 8), highlighting a clear acquisition from preferential interaction with the flysch formation (CAO). In the lower portion of the landslide (MS9) due to the differences in ^{87}Sr/^{86}Sr signature (Fig. 8) the interaction of groundwater with pure gypsum seems to be excluded; here, the high ^{87}Sr/^{86}Sr content is probably due to the dominantly interaction of groundwater with flysch (CAO), which outcrops extensively along the slope, and subordinately with the gypsum that is found in the landslide.

This hypothesis was also supported by the δ^{11}B results. The δ^{11}B value measured in MS9 falls in the field identified for limestone (Hemming and Hanson 1992), confirming that the interaction with the carbonatic component of the flysch formation is the main water–rock interaction process affecting groundwater in the lower portion of the landslide
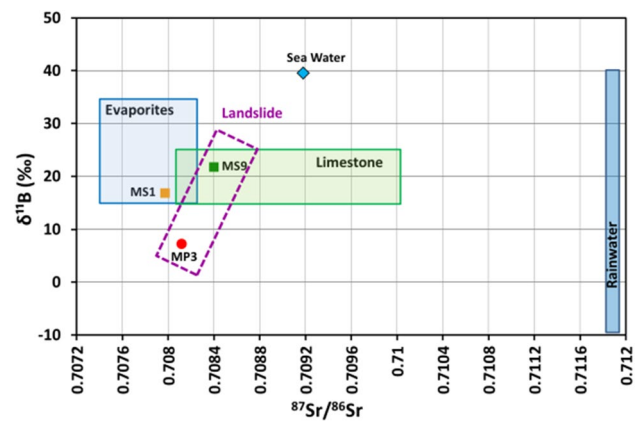
(Figs. 9, 10). Moreover, the similarity of the MS9 δ^{11}B value to the gypsum field (Lemarchand and Gaillardet 2006; Mao et al. 2019) confirms the subordinate interaction with gypsum that likely outcrops in the landslide body as small lenses or blocks. In the central portion of the landslide, the δ^{11}B value measured in MP3 suggests that water–rock interaction processes involve only the flysch formation, and allow to exclude the presence of gypsum in this portion of the landslide body and the bedrock (Figs. 9, 10). The lower δ^{11}B value found in this point is likely due to the presence in the central portion of the landslide of a silicatic component that generally imparts to groundwater a low isotopic signature (Barth 2000; Pennisi et al. 2000; Lemarchand and Gaillardet 2006; Millot and Négrel 2007).

As supported by isotopic analyses, gypsum blocks found inside the landslide, due to their small dimension seem to play a negligible role in the landslide stability. Accordingly rainfall infiltration and groundwater paths result to be the main parameter in the kinematics of the Montecagno landslide.

Conclusions

In the Montecagno landslide, a comprehensive study of chemical and multi-isotope analyses (δ^{18}O-δ^{2}H, ^{3}H, ^{87}Sr/^{86}Sr, δ^{11}B), groundwater level monitoring and hydrological lump modelling (FLOWPC) were performed to define the groundwater origin, flow paths, turnover time and bedrock lithology. In the study area, Triassic gypsum outcrops are quite widespread and composes the bedrock of the landslide deposits; the gypsum outcrops have serious consequences on the stability of the landslide deposits since

Fig. 10 Conceptual model of the Montecagno slope and landslide showing the schematic groundwater flow path. Blue squares represent piezometer; green square represents drain system; red squares represent inclinometers; blue circle and arrow represents MS1 spring that is not in line with the cross section; continuous light blue arrows represent the local rainfall infiltration along the slope; continuous blue arrows represent the flow path occurring in the landslide. The ^{3}H and δ^{11}B contents are reported near the corresponding sampling points as well tritium content of rainfall. The ^{87}Sr/^{86}Sr content detected in landslide is also reported
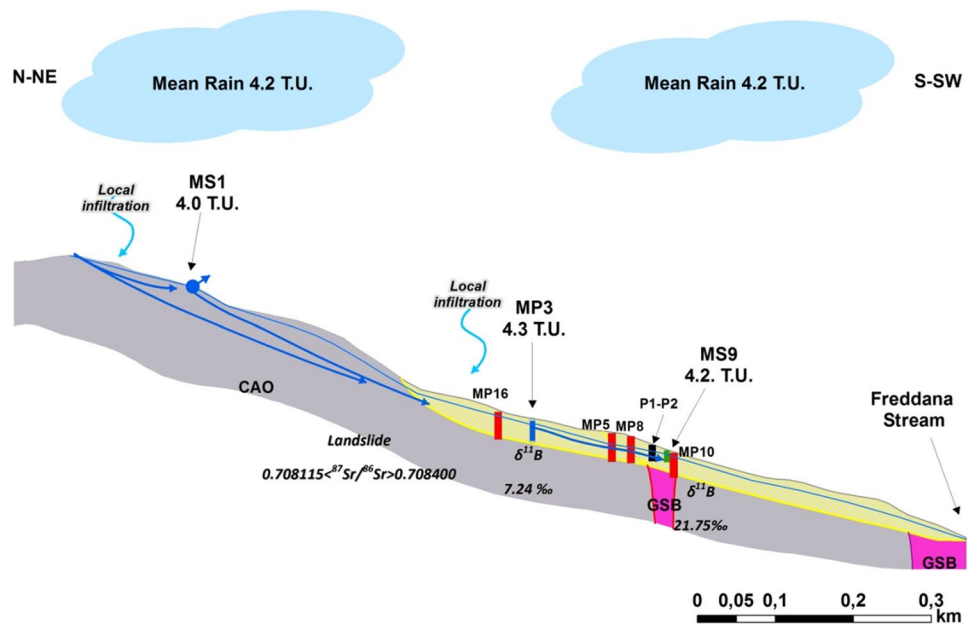
gypsum formations are affected by dissolution phenomena that can produce caves and collapses.

The results from the δ^{18}O-δ^2H and ^{3}H analyses and the δ^{18}O-elevation relationship suggest that the groundwater hosted inside the landslide has a recharge controlled by local rainwater. Groundwater inside the landslide is hosted in shallow flow paths. FLOWPC models suggest that in these flow paths, groundwater renewal occurs every 3–4 months.

Chemical analyses support a water–rock interaction with gypsum inside the slope; ^{87}Sr/^{86}Sr and δ^{11}B allow to confirm this hypothesis and obtain important information about the bedrock structures. Groundwater inside the central portion of the landslide is characterized by interaction with the flysch formation. In the lower portion of the landslide, the groundwater interacts primarily with flysch and subordinately with gypsum that is present in this portion of the slope as small lenses or blocks.

The small dimensions of the gypsum blocks allow us to hypothesize that the investigated portion of the Montecagno landslide is characterized by a low possibility of the occurrence of collapse phenomena and that groundwater infiltration play a key role in the landslide stability.

This research demonstrates that the methodology used, based on isotopic investigations, chemistry, modelling and groundwater level monitoring, can contribute to improving knowledge about the lithology of structures that are not visible with surface-based geological investigations and about the hydrogeological aspects of these rocks and the other adjacent formations.

References

Barth SR (2000) Geochemical and boron, oxygen and hydrogen isotopic constraints on the origin of salinity in groundwaters from the crystalline basement of the Alpine Foreland. Appl Geochem 15:937–952. https://doi.org/10.1016/S0883-2927(99)00101-8

Bogaard TA, Guglielmi Y, Marc V, Emblanch C, Bertrand C, Mudry J (2007) Hydrogeochemistry in landslide research: a review. Bull Soc Géol Fr 178:113–126. https://doi.org/10.2113/gssgfbull.178.2.113

Buchignani V, Avanzi GD, Giannecchini R, Puccinelli A (2008) Evaporite karst and sinkholes: a synthesis on the case of Camaiore (Italy). Environ Geol 53:1037–1044. https://doi.org/10.1007/s00254-007-0730-x

Calligaris C, Devoto S, Zini L (2017) Evaporite sinkholes of the Friuli Venezia Giulia region (NE Italy). J Maps 13(2):406–414. https://doi.org/10.1080/17445647.2017.1316321

Celle-Jeanton H, Travi Y, Blavoux B (2001) Isotopic typology of the precipitation in the western Mediterranean region at three different time scales. Geophys Res Lett 28(7):1215–1218. https://doi.org/10.1029/2000GL012407

Cervi F, Ronchetti F, Martinelli G, Bogaard T, Corsini A (2012) Origin and assessment of deep groundwater inflow in the Ca' Lita landslide using hydrochemistry and in situ monitoring. Hydrol Earth Syst Sci 16:4205–4221. https://doi.org/10.5194/hess-16-4205-2012

Cervi F, Borgatti L, Martinelli G, Ronchetti F (2014) Evidence of deep water inflow in a tectonic window of the northern Apennines (Italy). Environ Earth Sci 72(7):2389–2409. https://doi.org/10.1007/s12665-014-3149-1

Cervi F, Ronchetti F, Doveri M, Mussi M, Marcaccio M, Tazioli A (2016) The use of stable water isotopes from rain gauges network to define the recharge areas of springs: problems and possible solutions from case studies in the northern Apennines. Geoing Ambient Min 149:19–26

Chiesi M, Forti P (2009) L'alimentazione delle fonti di Poiano. Mem Istit Ital Speleol 22:69–98

Chiesi M, De Waele J, Forti P (2010) Origin and evolution of a salty gypsum/anhydrite karst spring: the case of Poiano (Northern Apennines, Italy). Hydrogeol J 18(5):1111–1124

Colombetti A, Fazzini P (1987) Idrogeologia carsica nella formazione di Burano nell'alta valle del F. Secchia. Atti Soc Nat Mat Di Modena 118:93–113

Corsini A, Berti M, Monni A, Pizziolo M, Bonacini F, Cervi F, Ciccarese G, Ronchetti F, Bertacchini E, Capra A, Gallucci A, Generali M, Gozza G, Pancioli V, Pignone S, Truffelli G (2013) Rapid assessment of landslide activity in Emilia Romagna using GB-InSAR short surveys. In: Margottini C, Canuti P, Sassa K (eds) Landslide science and practice. Springer, Berlin, pp 391–399

Craig H (1961) Isotopic variations in meteoric waters. Science 133:1702–1703. https://doi.org/10.1126/science.133.3465.1702

Cruden DM, Varnes DJ (1996) Landslide investigation and mitigation, transportation research board. Landslide types and process, National Research Council, National Academy Press, Special Report 247:36–75. https://onlinepubs.trb.org/Onlinepubs/sr/sr247/sr247-003.pdf.

De Montety V, Marc V, Emblanch C, Malet JP, Bertrand C, Maquaire O, Bogaard T (2007) Identifying origin of groundwater and flow processes in complex landslides affecting black marls in southern French Alps: insights from a hydrochemical survey. Earth Surf Process Landf 32:32–48. https://doi.org/10.1002/esp.1370

Deiana M (2017) Stable and unstable groundwater isotopes applied to deep-seated landslides. PhD Thesis, University of Modena and Reggio Emilia, Modena, Italy

Deiana M, Ronchetti F, Mussi M (2016) 2014–2015 Tritium values in small and shallow aquifers in northern Apennines. EGU General Assembly 2016, vol 18, Vienna, April 2016

Deiana M, Mussi M, Ronchetti F (2017) Discharge and environmental isotope behaviours of adjacent fractured and porous aquifers. Environ Earth Sci 76:595. https://doi.org/10.1007/s12665-017-6897-x

Deiana M, Cervi F, Pennisi M, Mussi M, Bertrand C, Tazioli A, Corsini A, Ronchetti F (2018) Chemical and isotopic investigations ($\delta^{18}O$, δ^2H, ^3H, $^{87}Sr/^{86}Sr$) to define groundwater processes occurring in a deep-seated landslide in flysch. Hydrogeol J 26(3):2669–2691. https://doi.org/10.1007/s10040-018-1807-1

Denchik N, Gautier S, Dupuy M, Batiot-Guilhe C, Lopez M, Léonardi V, Geeraert M, Henry G, Neyens D, Coudray PA, Pezard PA (2019) In-situ geophysical and hydro-geochemical monitoring to infer landslide dynamics (Pégairolles-de-l'Escalette landslide, France). Eng Geol 254:102–112. https://doi.org/10.1016/j.enggeo.2019.04.009

Dinelli E, Testa G, Cortecci G, Barbieri M (1999) Stratigraphic and petrographic constraints to trace element and isotope geochemistry of Messinian sulfates of Tuscany. Mem Soc Geol Ital 54:61–74

Doveri M, Mussi M (2014) Water isotopes as environmental tracers for conceptual understanding of groundwater flow: an application for fractured aquifer systems in the "Scansano-Magliano in Toscana" area (Southern Tuscany, Italy). Water 6(8):2255–2277

Duchi V, Venturelli G, Boccasavia I, Bonicolini F, Ferrari C, Poli D (2005) Studio geochimico dei fluidi dell'Appennino Tosco-Emiliano-Romagnolo. Boll Soc Geol Ital 124:475–491

Elderfield H (1986) Strontium isotope stratigraphy. Palaeogeogr Palaeocl 57(1):71–90. https://doi.org/10.1016/0031-0182(86)90007-6

Elorza MG, Santolalla FG (1998) Geomorphology of the tertiary gypsum formations in the ebro depression (Spain). Geoderma 87(1–2):1–29. https://doi.org/10.1016/S0016-7061(98)00065-2

Fetter CW (1980) Applied hydrogeology. Prentice Hall, Englewood Cliffs, p 691

Forti P, Sauro U (1996) The gypsum karst of Italy. Int J Speleol 25(3/4):239–250

Gargini A, Vincenzi V, Piccinini L, Zuppi GM, Canuti P (2008) Groundwater flow systems in turbidites of the northern Apennines (Italy): natural discharge and high speed railway tunnel drainage. Hydrogeol J 16:1577–1599. https://doi.org/10.1007/s10040-008-0352-8

Gran G (1952) Determination of the equivalence point in the potentiometric titrations. Analyst 77:661–671. https://doi.org/10.1039/AN9527700661

Gutiérrez F (2010) Hazard associated with karst. In: Alcántara-Ayala I, Goudie AS (eds) Geomorphological hazards and disaster prevention. Cambridge University Press, Cambridge

Gutiérrez F, Cooper AH (2013) Surface morphology of gypsum karst. In: Frumkin A, Shroder J (eds) Treatise on geomorphology, vol 6, Karst geomorphology. Academic Press, San Diego

Hemming NG, Hanson GN (1992) Boron isotopic composition and concentration in modern marine carbonates. Geochim Cosmochim Acta 56:537–543. https://doi.org/10.1016/0016-7037(92)90151-8

Intrieri E, Gigli G, Nocentini M, Lombardi L, Mugnai F, Fidolini F, Casagli N (2015) Sinkhole monitoring and early warning: an experimental and successful GB-InSAR application. Geomorpology 241:304–314. https://doi.org/10.1016/j.geomorph.2015.04.018

Klimchouk A, Cucchi F, Calaforra JM, Aksem S, Finocchiaro F, Forti P (1996) Dissolution of gypsum from field observations. Int J Speleol 25:37–48. https://doi.org/10.5038/1827-806X.25.3.3

Koch GS, Link RF (1971) The coefficient of variation; a guide to the sampling of ore deposits. Econ Geol 66(2):293–301. https://doi.org/10.2113/gsecongeo.66.2.293

La Rosa A, Pagli C, Molli G, Casu F, De Luca C, Pieroni A, D'Amato Avanzi G (2018) Growth of a sinkhole in a seismic zone of the northern Apennines (Italy). Nat Hazards Earth Syst Sci 18:2355–2366. https://doi.org/10.5194/nhess-18-2355-2018

Lauber U, Goldscheider N (2014) Use of artificial and natural tracers to assess groundwater transit-time distribution and flow systems in a high-alpine karst system (Wetterstein Mountains, Germany). Hydrogeol J 22(8):1807–1824. https://doi.org/10.1007/s10040-014-1173-6

Lemarchand D, Gaillardet J (2006) Transient features of the erosion of shales in the Mackenzie basin (Canada), evidences from boron isotopes. Earth Planet Sci Lett 245:174–189. https://doi.org/10.1016/j.jseaes.2012.07.008

Longinelli A, Selmo E (2003) Isotopic composition of precipitation in Italy: a first overall map. J Hydrol 270:75–88. https://doi.org/10.1016/S0022-1694(02)00281-0

Lugli S (2001) Timing of post-depositional events in the Burano Formation of the Secchia valley Upper Triassic, Northern Apennines), clues from gypsum ± anhydrite transitions and carbonate metasomatism. Sedim Geol 140:107–122. https://doi.org/10.1016/S0037-0738(00)00174-3

Maloszewski P, Zuber A (2002) Manual on lumped parameter models used for the interpretation of environmental tracer data in groundwaters (IAEA-UIAGS/CD-02-00131). International Atomic Energy Agency (IAEA)

Mao HR, Liu CQ, Zhao ZQ (2019) Source and evolution of dissolved boron in rivers: insights from boron isotope signatures of end-members and model of boron isotopes during weathering processes. Earth Sci Rev 190:439–459. https://doi.org/10.1016/j.earscirev.2019.01.016

Marc V, Bertrand C, Malet JPh, Carry N, Simler R, Cervi F (2017) Groundwater-surface waters interactions at slope and catchment scales: implications for landsliding in clay-rich slopes. Hydrol Process 31(2):364–381. https://doi.org/10.1002/hyp.11030

Millot R, Négrel P (2007) Multi-isotopic tracing (δ^7Li, δ^{11}B, ^{87}Sr/^{86}Sr) and chemical geothermometry: evidence from hydro-geothermal systems in France. Chem Geol 244(664):678. https://doi.org/10.1016/j.chemgeo.2007.07.015

Millot R, Guerrot C, Innocent C, Negrel Ph, Sanjuan B (2011) Chemical, multi-isotopic (Li–B–Sr–U–H–O) and thermal characterization of Triassic formation waters from the Paris Basin. Chem Geol 283:22–241. https://doi.org/10.1016/j.chemgeo.2011.01.020

Mussi M, Leone G, Nardi I (1998) Isotopic geochemistry of natural water from the Alpi Apuane-Garfagnana area, Northern Tuscany, Italy. Mineral Petrogr Acta 41:163–178

Négrel P, Guerrot C, Millot R (2007) Chemical and strontium isotope characterization of rainwater in France: influence of sources and hydrogeochemical implications. Isot Environ Healt Stud 43:179–196. https://doi.org/10.1080/10256010701550773

Négrel P, Petelet-Giraud E, Brenot A (2009) Use of isotopes for groundwater characterization and monitoring. In: Fouillac AM, Grath MJ, Ward R (eds) Groundwater monitoring. Wiley, Oxford

Pennisi M, Gonfiantini R, Grassi S, Squarci P (2000) The utilization of boron and strontium isotopes for the assessment of boron contamination of the Cecina River alluvial aquifer (central-western Tuscany, Italy). Appl Geochem 21:643–655. https://doi.org/10.1016/j.apgeochem.2005.11.005

Sánchez-Murillo R, Brooks ES, Elliot WJ, Boll J (2015) Isotope hydrology and baseflow geochemistry in natural and human-altered watersheds in the Inland Pacific Northwest, USA. Isot Environ Health Stud 51(2):231–254. https://doi.org/10.1080/10256016.2015.1008468

Segadelli S, Vescovi P, Ogata Kchelli A, Zanini A, Boschetti T, Petrella E, Toscani L, Gargini A, Celico F (2017) A conceptual hydrogeological model of ophiolitic aquifers (serpentinised peridotite): the test example of Mt. Prinzera (Northern Italy). Hydrol Process 31(5):L1058–L1073. https://doi.org/10.1002/hyp.11090

Spötl C, Pak E (1996) A strontium and sulfur isotopic study of Permo-Triassic evaporites in the Northern Calcareous Alps, Austria. Chem Geol 131:219–234. https://doi.org/10.1016/0009-2541(96)00017-4

Tazioli A, Cervi F, Doveri M, Mussi M, Deiana M, Ronchetti F (2019) Estimating the isotopic altitude gradient for hydrogeological studies in mountainous areas: are the low-yield springs suitable? Insights from the Northern Apennines of Italy. Water 11(9):1764

Thornthwaite CW, Mater JR (1957) Instruction and tables for computing potential evapotranspiration and the water balance. Publ Clim 10:185–311

Toscani L, Venturelli G, Boschetti T (2001) Sulphide-bearing waters in northern Apennines, Italy: general features and water-rock interaction. Aquat Geochem 7:195–216

Vallet A, Bertrand C, Mudry J, Bogaard T, Fabbri O, Baudement C, Régent B (2015) Contribution of time-related environmental tracing combined with tracer tests for characterization of a groundwater conceptual model: a case study at the Séchilienne landslide, Western Alps (France). Hydrogeol J 23:1761–1779. https://doi.org/10.1007/s10040-015-1298-2

Vespasiano G, Apollaro C, De Rosa R, Muto F, Larosa S, Fiebig J, Mulch A, Marini L (2015) The small spring method (SSM) for the definition of stable isotope–elevation relationships in northern Calabria (southern Italy). Appl Geochem 63:333–346. https://doi.org/10.1016/j.apgeochem.2015.10.001

Viville D, Ladouche B, Bariac T, T. (2006) Isotope hydrological study of mean transit time in the granitic Strengbach catchment (Vosges massif, France): application of the FlowPC model with modified input function. Hydrol Process 20(8):1737–1751

Xiao J, Xiao YK, Jin ZD, He MY, Liu CQ (2013) Boron isotope variations and its geochemical application in nature. Aust J Earth Sci 60:431–447. https://doi.org/10.1080/08120099.2013.813585

Yılmaz I (2001) Gypsum/anhydrite: some engineering problems. Bull Eng Geol Environ 59:227–230. https://doi.org/10.1007/s100640000071